

Article

SnO₂ Composite Films for Enhanced Photocatalytic Activities

Ke Han ¹, Xue-Lei Peng ², Fang Li ¹ and Ming-Ming Yao ^{1,*}

¹ Key Laboratory of Interfacial Reaction & Sensing Analysis in Universities of Shandong, School of Chemistry and Chemical Engineering, University of Jinan, Jinan 250022, China; xjs5836179@163.com (K.H.); chm_lif@ujn.edu.cn (F.L.)

² Jinan Institute of Product Quality Inspections, Jinan 250022, China; pxl_JN@126.com

* Correspondence: chm_yaomm@ujn.edu.cn; Tel.: +86-531-8276-5959; Fax: +86-531-8276-5969

Received: 7 September 2018; Accepted: 8 October 2018; Published: 14 October 2018



Abstract: As a new type of promising semiconductor photocatalyst, SnO₂ cannot be widely applied due to its low utilization efficiency to visible light and swift recombination of photogenerated electrons and holes. These drawbacks were effectively overcome by preparing the B/Ag/F tridoped SnO₂-ZnO composite films using the simple sol-gel method. The degradation of the methyl green and formaldehyde solutions was used to value the photocatalytic activity of the samples. Photoluminescence (PL) spectra and the UV-Vis absorption spectroscopy results of the samples illustrated that the B/Ag/F tridoped SnO₂-ZnO composite film not only improved the lifetime of the charge carriers, but also enhanced their visible light absorption. The X-ray diffraction (XRD) results showed that the crystalline SnO₂ was in the structure of rutile. As exhibited in the BET surface area results, the specific surface area of pure SnO₂ was 19.9 m²g⁻¹, while that of the B/Ag/F tridoped SnO₂-ZnO was 85.3 m²g⁻¹. Compared to pure SnO₂, SnO₂-ZnO, or the mono- or di-doped SnO₂-ZnO films, the B/Ag/F tridoped SnO₂-ZnO composite film had the highest photocatalytic activity.

Keywords: SnO₂-ZnO film; B/Ag/F tridoping; photodegradation

1. Introduction

Drinking water is one of our most precious resources. However, fresh water is frequently contaminated with industrial wastewater. Water pollution brought by all kinds of contaminants has become a threat to our health [1,2]. In recent years, much attention has been drawn towards the control of organic pollutants from industrial wastewater [3]. The photodegradation of organic wastewater by irradiated semiconductor photocatalysts has already proven to be a fruitful process [4–7], which can lead to completely converting the pollutants into water and carbon dioxide.

In the past few decades, SnO₂ has become a potential photocatalyst applied to the treatment of organic wastewater due to its nontoxic nature, low cost of production, and chemical stability [8]. The photocatalytic activity mainly depends on two factors: (1) the production of photo-generated electrons (e⁻) and holes (h⁺); and (2) the effective separation ability of the e⁻/h⁺ pairs [9,10]. The band gap of SnO₂ is 3.6 eV, so SnO₂ is only irradiated by UV light to bring about the transition of electrons from the valence band to the conduction band, hence generating holes in the valence band [11]. Furthermore, the species is very unstable, and the recombination of electrons and holes can occur quickly. To overcome these drawbacks, composite semiconductors and metal or nonmetal doping techniques were proposed to improve the photocatalytic activity of SnO₂ [12,13]. Composite semiconductors have been widely applied as a quite simple and highly effective approach for basic photocatalyst modification [14]. Compared to pure SnO₂, the photocatalytic performance of coupled SnO₂-ZnO is better. The increased charge separation caused by the SnO₂-ZnO coupling leads to the enhancement of the photocatalytic activity of the catalysts [15].

Ion doping has also been used in photocatalyst modification. It was reported that B ions can narrow their band gap by being incorporated into SnO₂ lattices [12]. When incorporated into the metal oxide structures, the Ag ions can act as electron traps to effectively transfer the photogenerated electrons of metal oxides and act as electron sinks [16,17]. The ionic radius of O²⁻ is similar to that of F⁻, and the Sn-O bond is highly comparable to that of the Sn-F bond. Therefore, the F ions can replace the O in the lattice of tin dioxide to generate more holes in the crystal [18]. Compared with single doping, the co-doping of metals and nonmetals has shown superior photocatalytic activity [19]. In general, energy levels of metal doping are lower than the conduction band of the semiconductor, while those of nonmetal doping are higher than the valence band of the semiconductor. Therefore, low-content co-doping with metal and nonmetal ions can effectively narrow the band gap so as to enhance the photocatalytic activity of metal oxide. These points indicate that the B/Ag/F tridoping and ZnO compositing may be an effective way to improve the photocatalytic activity of SnO₂ photocatalyst.

In the present work, a B/Ag/F tridoped SnO₂-ZnO composite film was prepared through a simple sol-gel method. We tested the photocatalytic activities of the catalyst in organic pollutant solutions including methyl green (MG) and formaldehyde. The photodegradation efficiency was significantly enhanced due to the synergic effects of ZnO compositing and the B/Ag/F tridoping. To the best of our knowledge, there have been few studies concentrating on B/Ag/F tridoped SnO₂-ZnO composite films for the photodegradation of organic pollution in aqueous solutions.

2. Results and Discussion

2.1. Photocatalytic Activity

Methyl green, as a typical organic dye, is released into the natural environment after being used in the printing and textile industries. Because of its potential carcinogenicity, the removal of methyl green from wastewater has been a matter of considerable interest. Figure 1 exhibits the ultraviolet-visible absorption spectra (a) and the degradation rate (b) of the methyl green solutions employing SnO₂, SnO₂-ZnO, B doped SnO₂-ZnO, B/Ag di-doped SnO₂-ZnO, and B/Ag/F tridoped SnO₂-ZnO films under UV (wavelength of 365 nm) irradiation for 45 min. As shown in Figure 1b, the degradation percentage of the methyl green solutions using a pure SnO₂ film was about 26%, compared with SnO₂-ZnO (32%), B doped SnO₂-ZnO (41%), B/Ag di-doped SnO₂-ZnO (45%), and B/Ag/F tridoped SnO₂-ZnO films (51%). It can be seen that the photodegradation rate of the B/Ag/F tridoped SnO₂-ZnO film was the highest among all the samples.

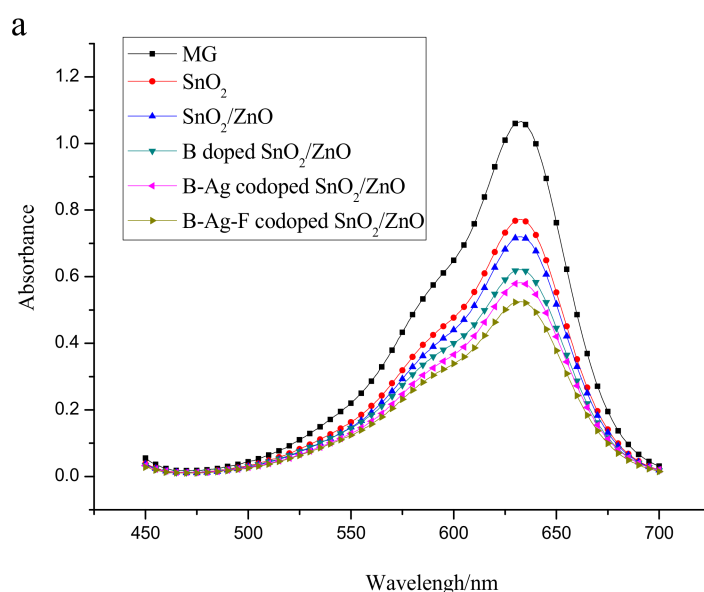


Figure 1. Cont.

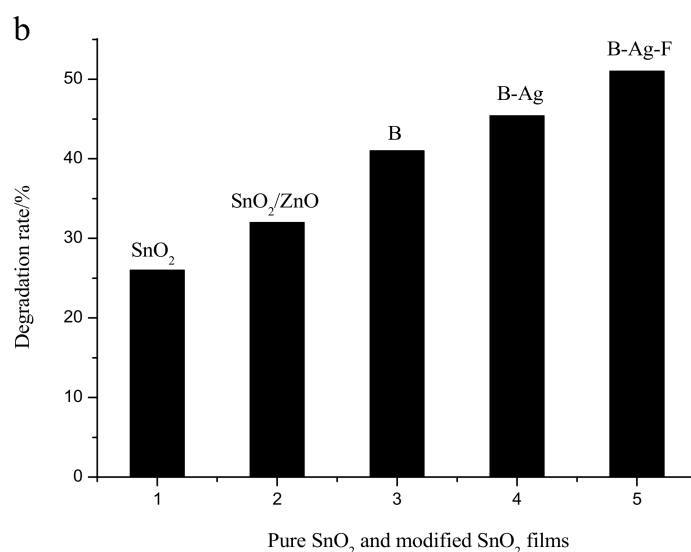


Figure 1. The (a) ultraviolet–visible absorption spectra and (b) degradation percentage of the methyl green (MG) solutions using pure SnO₂, SnO₂–ZnO, B doped SnO₂–ZnO, B/Ag di-doped SnO₂–ZnO, and B/Ag/F tridoped SnO₂–ZnO films under UV irradiation for 45 min.

To further evaluate the photocatalytic activity of the samples, the photodegradation rate of the methyl green or formaldehyde solutions was evaluated under visible irradiation. Figure 2 illustrates the decomposition kinetics of the methyl green (a) and formaldehyde solutions (b) employing SnO₂, SnO₂–ZnO, and B/Ag/F tridoped SnO₂–ZnO films under visible irradiation for 120 min. It is observed in Figure 2a that the degradation rate of the methyl green solutions employing the B/Ag/F tridoped SnO₂–ZnO film was the highest of all the samples, and reached 54% in the allotted time, while those of pure SnO₂ and SnO₂–ZnO were only 25% and 34%, respectively. Formaldehyde is a carcinogen, and is a common organic pollutant that is very frequently detected in wastewater. As exhibited in Figure 2b, the degradation percentages of the formaldehyde solutions employing pure SnO₂, SnO₂–ZnO, and B/Ag/F tridoped SnO₂–ZnO films were 21%, 42%, and 60%, respectively. Based on the above experiments, we can draw the conclusion that the B/Ag/F tridoped SnO₂–ZnO film had the highest photocatalytic activity among all the samples under both UV and visible light irradiation. Moreover, the B/Ag/F tridoped SnO₂–ZnO photocatalyst was effective in degrading organic dyes and volatile organic pollutants.

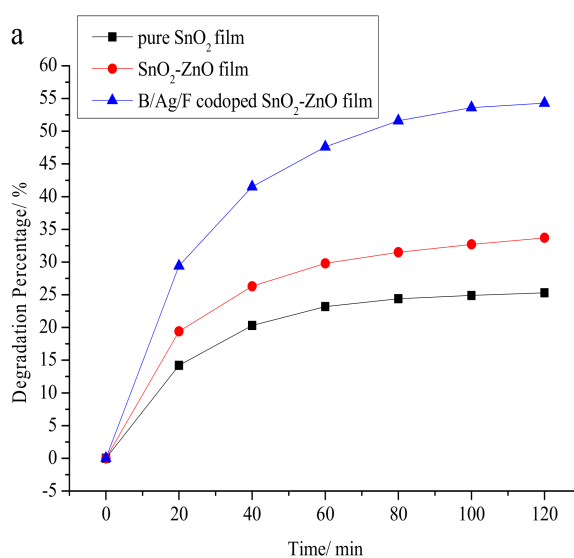


Figure 2. Cont.

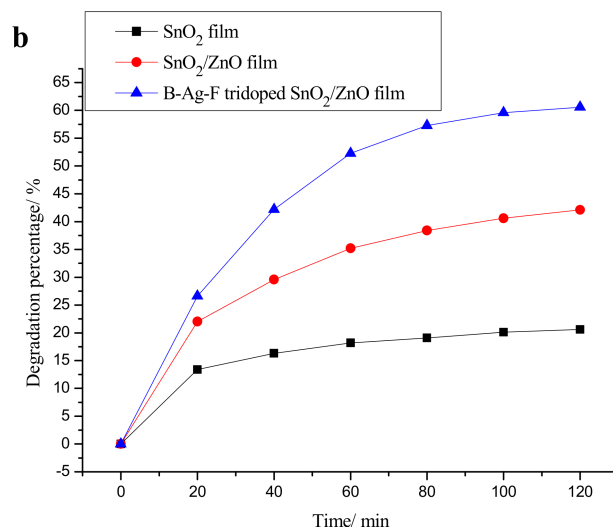


Figure 2. The decomposition kinetics of the (a) methyl green and (b) formaldehyde solutions employing pure SnO₂, SnO₂-ZnO, and B/Ag/F tridoped SnO₂-ZnO films under visible irradiation for 120 min.

Figure 3 shows the composition of the B/Ag/F tridoped SnO₂-ZnO film by energy dispersive spectroscopy (EDS, X-Max 20, Oxford, Britain). The weight concentrations (%) of Sn, Zn, B, Ag, F, O, and C in the film were 63.01, 0.95, 1.28, 2.34, 0.82, 25.65 and 5.96, respectively. Carbon may come from residual organic matter or the instrument itself.

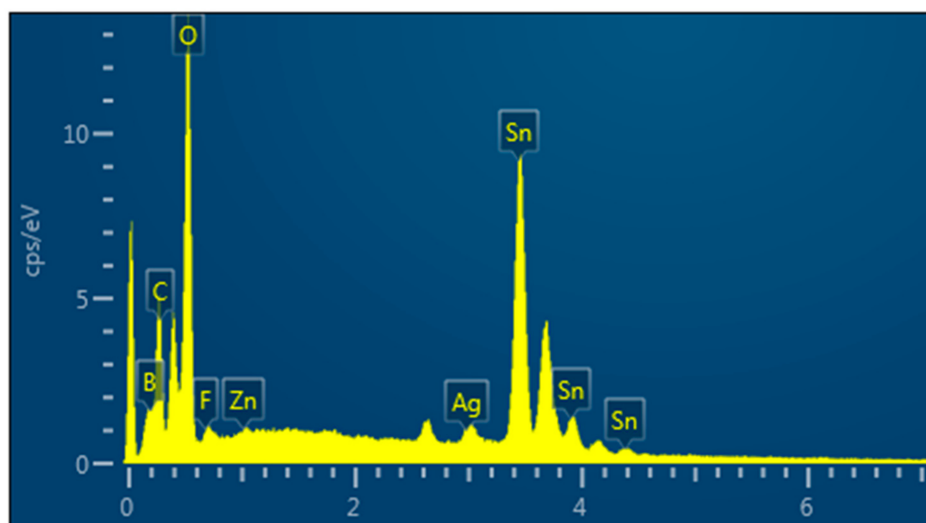


Figure 3. Energy dispersive spectroscopy (EDS) of the B/Ag/F tridoped SnO₂-ZnO film.

2.2. Optical Absorption

The optical properties of the semiconductors significantly determine their photocatalytic performance. Figure 4 shows the ultraviolet visible absorption spectra (a) and $(\alpha h\nu)^{1/2}$ vs. $h\nu$ plots (b) of SnO₂, SnO₂-ZnO, and B/Ag/F tridoped SnO₂-ZnO films. A red shift of the absorption edge was clearly seen for the B/Ag/F tridoped SnO₂-ZnO film. The band gap of the semiconductors can be acquired using the following formula $\alpha h\nu = A(h\nu - E_g)^{n/2}$, where α , h , ν , A , E_g are absorption coefficient, Planck's constant, light frequency, proportional constant, and energy band gap, respectively. The value of n , a constant, is determined by the type of a semiconductor [20]. Therefore, a plot of $(\alpha h\nu)^{1/2}$ versus energy ($h\nu$) can be used to determine the band gap energy of the films. As shown in Figure 4b, the band gaps of pure SnO₂, SnO₂-ZnO, and B/Ag/F tridoped SnO₂-ZnO films were 3.35,

3.05, and 2.1 eV, respectively. The low band gap can play a significant role in the photocatalytic activity of the catalysts because photons with lower energy can be active in the photocatalytic reactions.

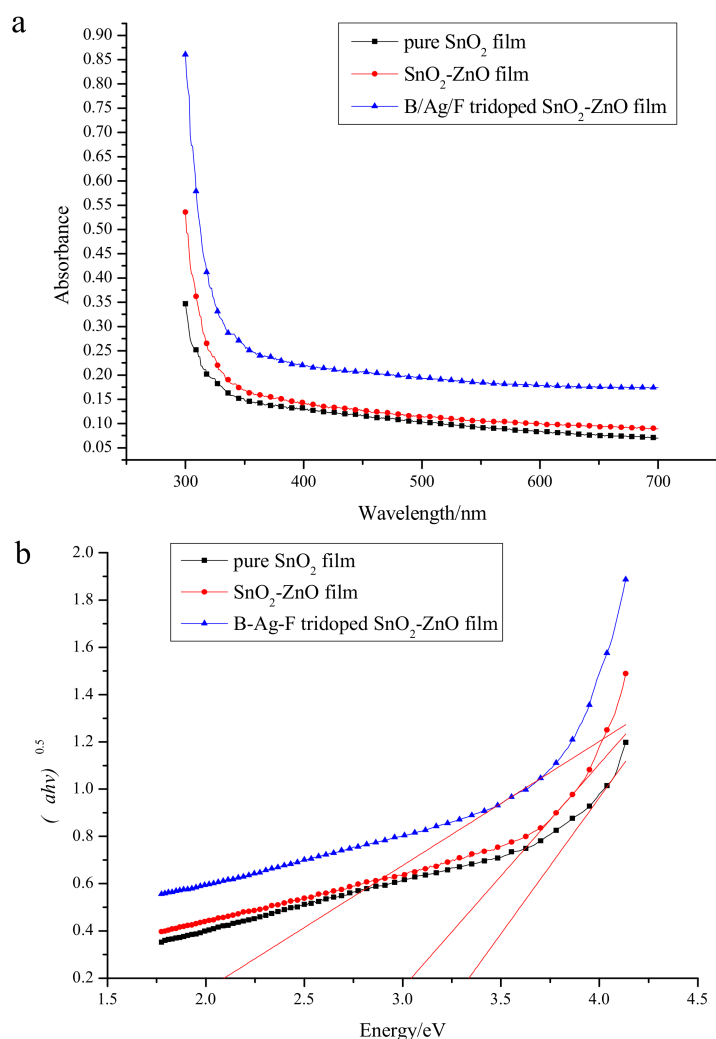


Figure 4. The (a) ultraviolet–visible absorption spectra and (b) $(\alpha h\nu)^{1/2}$ vs. $h\nu$ plots of SnO₂, SnO₂-ZnO, and B/Ag/F tridoped SnO₂-ZnO films.

2.3. Photoluminescence (PL) Analysis

As illustrated in Figure 5, the PL spectra (FLS920, Edinburgh, UK) of pure SnO₂, SnO₂-ZnO, and B/Ag/F tridoped SnO₂-ZnO films, using a 300 nm line of 450 W xenon lamps as excitation source, were applied to investigate the recombination rate of the photogenerated electron–hole pairs [21]. Although the intensities of the samples were different, their peak positions (380 nm) were the same. The B/Ag/F tridoped SnO₂-ZnO film had the lowest emission peak intensity among the three samples, indicating the highest transfer efficiency and lowest recombination rate of the electron–hole pairs [22], thus enhancing the photocatalytic activity of the B/Ag/F tridoped SnO₂-ZnO film.

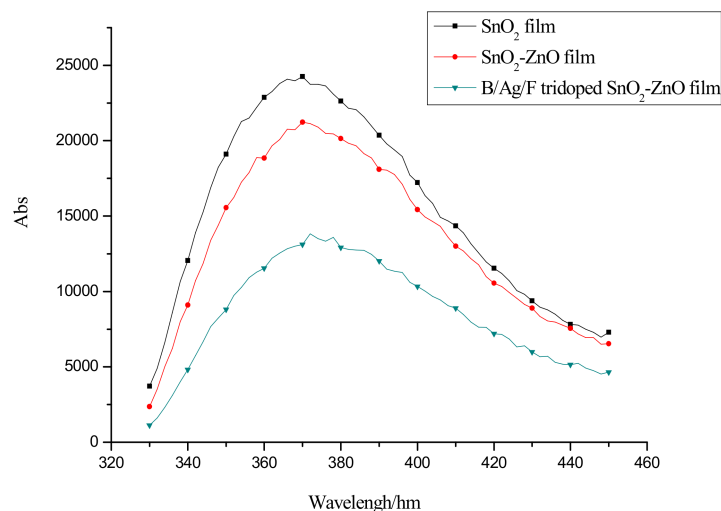


Figure 5. Photoluminescence (PL) spectra of pure SnO₂, SnO₂-ZnO, and B/Ag/F tridoped SnO₂-ZnO films.

2.4. Crystal Structure

The crystal structure of SnO₂ is significantly related to its photocatalytic activity. Figure 6 shows XRD patterns of pure SnO₂, SnO₂-ZnO, and B/Ag/F tridoped SnO₂-ZnO samples heated at 550 °C in atmosphere for 1 h. The patterns exhibited typical diffraction peaks at $2\theta = 26.6^\circ$, 33.9° , 37.9° , 51.8° , 54.8° , and 57.8° , which were assigned to the (110), (101), (200), (211), (220), and (002) planes of the rutile phase of SnO₂, respectively [23]. No obvious B, Ag, or F ions' related compound peaks were presented, indicating that the small amounts of dopants were uniformly scattered on SnO₂. No diffraction peak of ZnO was observed because the coupling amount of ZnO in the SnO₂-ZnO systems was very small or the peaks of SnO₂ were so strong that the weak peaks of ZnO were covered [19]. Compared to pure SnO₂ or SnO₂-ZnO, the B/Ag/F tridoped SnO₂-ZnO sample had broader and weaker diffraction peaks, indicating its smaller crystal sizes. According to the Scherrer formula, $d = 0.9\lambda / \beta \cos\theta$, the average size of the B/Ag/F tridoped SnO₂-ZnO particles was 4.8 nm, while that of pure SnO₂ and SnO₂-ZnO particles was 13.6 and 10.2 nm, respectively. Catalysts composed of smaller particles or crystal size are more effective in degrading organic pollutants.

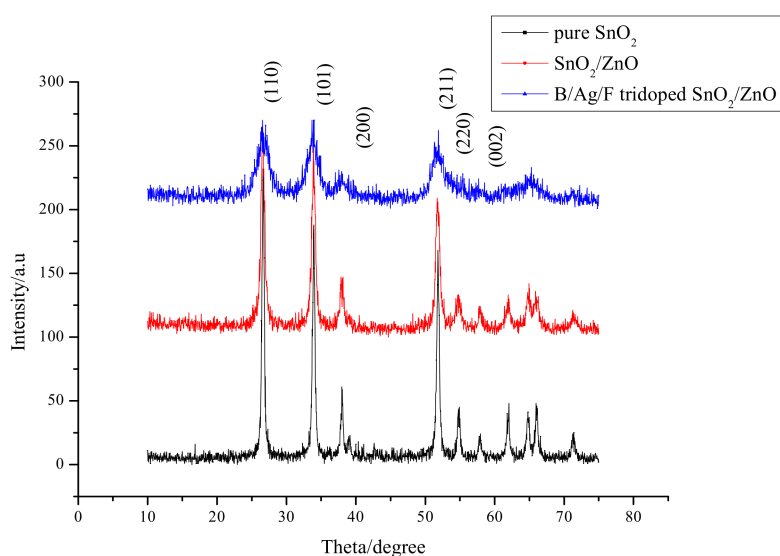


Figure 6. XRD patterns of pure SnO₂, SnO₂-ZnO, and B/Ag/F tridoped SnO₂-ZnO samples heated at 550 °C in atmosphere for 1 h.

2.5. Thermal Analysis

The differential thermal analysis–thermogravimetry (DTA-TG) curves for SnO₂ (a), SnO₂-ZnO (b), and B/Ag/F tridoped SnO₂-ZnO (c) powders within the range of 30–650 °C are shown in Figure 7. As shown in the TG curves, the mass losses of the three samples were extremely fast before 400 °C with the increase of temperature, but their weights had nearly no change after 400 °C. The DTA curves of the three samples showed three analogous strong endothermic peaks and one analogous exothermic peak. The two endothermic peaks at 85–90 °C and 161–173 °C, respectively, were due to the evaporation of water and ethanol. The endothermic peak at 235–254 °C is attributed to the loss of crystal water. As shown in Figure 7a, the exothermic peaks for the pure SnO₂ sample at 362.9 and 427.3 °C may be caused by the crystallization of SnO₂ [24]. From Figure 7b,c, the exothermic peaks at 384.5 and 398.1 °C are mainly due to the complete recrystallization of SnO₂ and ZnO.

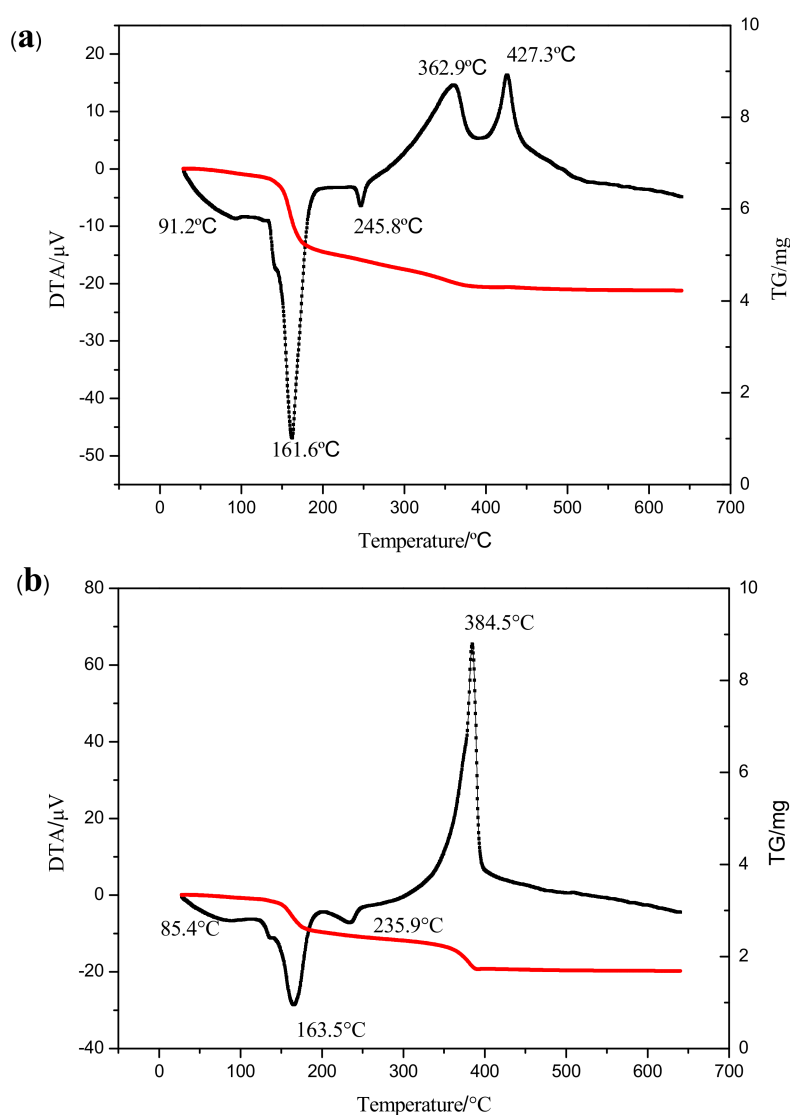


Figure 7. Cont.

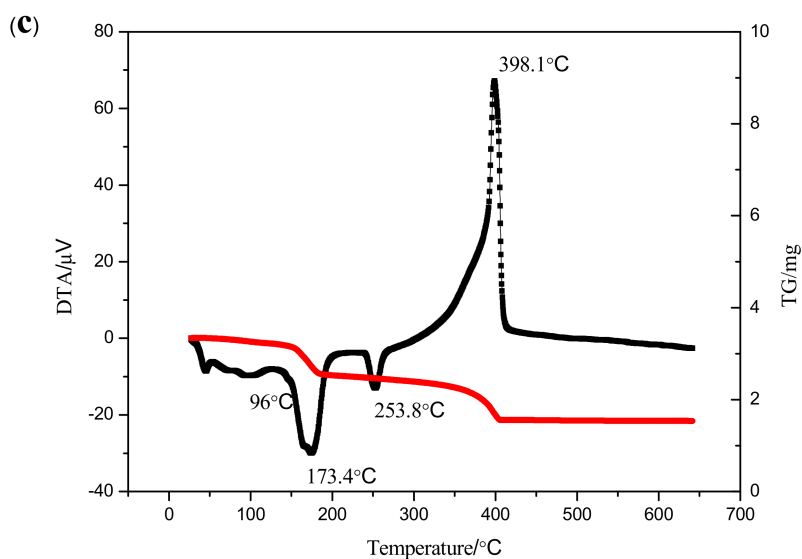


Figure 7. Differential thermal analysis–thermogravimetry (DTA-TG) curves for (a) pure SnO₂; (b) SnO₂-ZnO; and (c) B/Ag/F tridoped SnO₂-ZnO powders within the range 30–650 °C.

2.6. Surface Areas

Specific surface area is a critical factor for photocatalysts. Figure 8 shows the N₂ adsorption/desorption isotherms (a) and pore size distribution (b) of pure SnO₂ and B/Ag/F tridoped SnO₂-ZnO powders heated at 550 °C in atmosphere for 1 h. As shown in Figure 8a, the specific surface area of pure SnO₂ was 19.9 m²/g, while that of B/Ag/F tridoped SnO₂-ZnO was 85.3 m²/g at the same relative pressure. The enhancement of specific surface area may be assigned to the reduced particle size attributed to the addition of the B/Ag/F ions and ZnO into the SnO₂ film. From Figure 8b, the pore size of pure SnO₂ was 12 nm, while that of the B/Ag/F tridoped SnO₂-ZnO was only 5 nm. The decrease in average pore size caused by the B/Ag/F tridoping and ZnO compositing may be mainly due to the factor that the B/Ag/F ions or ZnO can be inserted in the pores of SnO₂, leading to smaller pore size. The smaller pore size and the larger specific surface areas can effectively adsorb O₂, H₂O, and contaminants, thus improving the photocatalytic property of the catalyst.

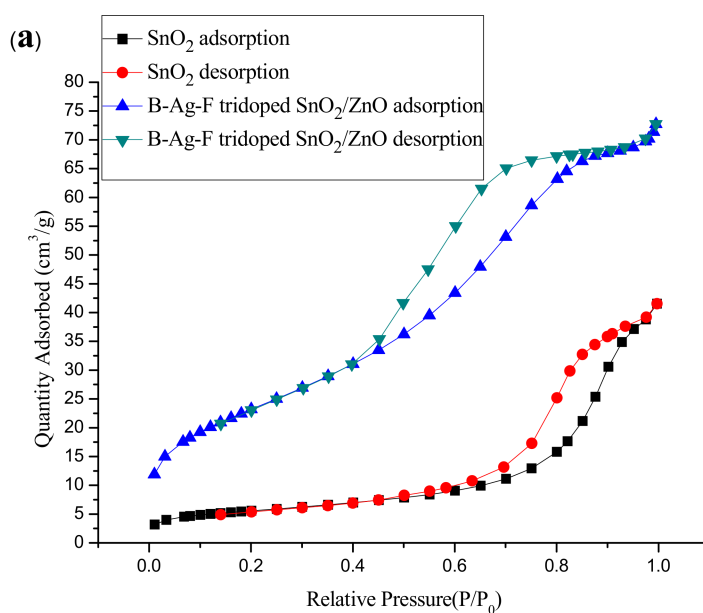


Figure 8. Cont.

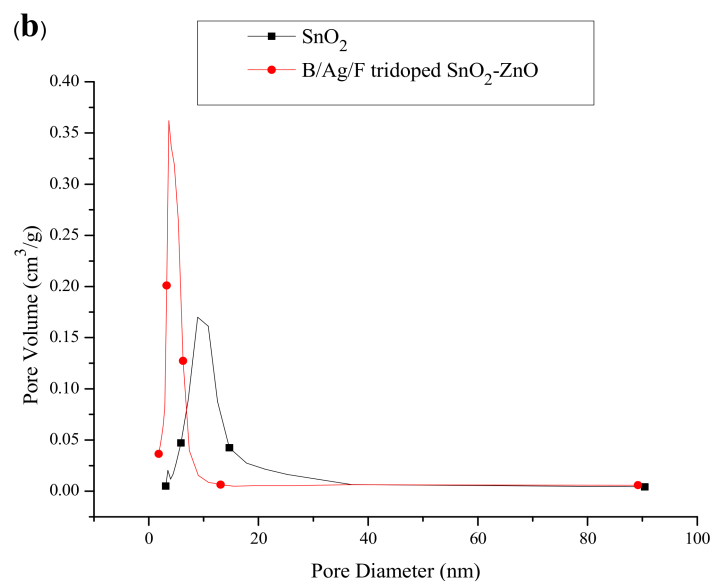


Figure 8. (a) N₂ adsorption/desorption isotherms and (b) pore size distribution of pure SnO₂ and B/Ag/F tridoped SnO₂-ZnO powders heated at 550 °C in atmosphere for 1 h.

2.7. Surface Morphology

The photocatalytic activity of the catalyst is often affected by its surface morphology. The field emission SEM (FE-SEM) images for SnO₂ (a) and B/Ag/F tridoped SnO₂-ZnO (b) are shown in Figure 9. It is obvious that the B/Ag/F tridoped SnO₂-ZnO film with no cracks was made up of smaller particles or aggregates compared to the SnO₂ film. As is well-known, a good dispersion or decreased aggregation among particles can lead to an active reactant contact area, and the photocatalytic activity of the catalyst may be enhanced.

In a word, the B/Ag/F tridoped SnO₂ film showed the highest photocatalytic activity for the degradation of organic pollutants among all the samples due to the synergistic effects caused by the B/Ag/F tridoping and ZnO compositing. The synergistic effects may provide ideal conditions for the charges to be photogenerated, separated, and transferred to the surface [25].

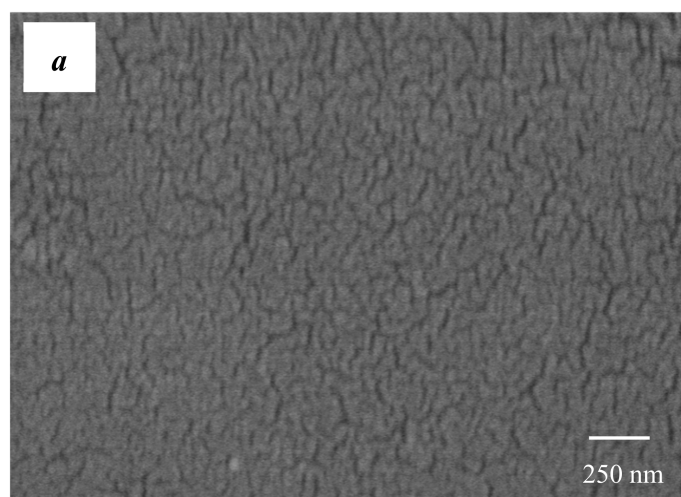


Figure 9. Cont.

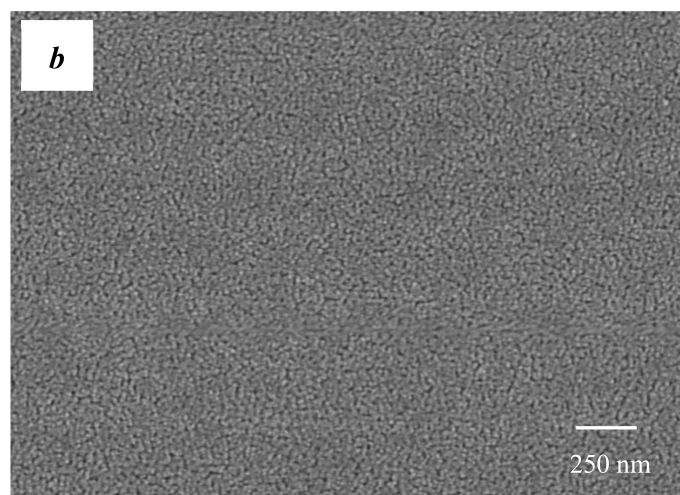


Figure 9. Field emission SEM (FE-SEM) images for (a) SnO₂ and (b) B/Ag/F tridoped SnO₂-ZnO heated at 550 °C in the atmosphere for 1 h.

3. Experimental

3.1. Film Preparation

We used analytical-grade chemicals throughout our study. SnCl₂·2H₂O, Zn(CH₃COO)₂·2H₂O, and C₂H₅OH were supplied by Sinopharm Chemical Reagent Limited Company (Beijing, China). Other chemicals were supplied by Jinan Chemical Reagent Factory (Jinan, China).

SnO₂ sol or ZnO sol was prepared through the sol-gel method [12,20]. We added 12.64 g SnCl₂·2H₂O to 80 mL of anhydrous ethanol in a beaker. Then, the solution was stirred for 30 min by a magnetic stirrer. SnO₂ sol could be obtained after three days of aging at room temperature. To prepare zinc acetate ethanol solution (A solution), 0.0988 g Zn(CH₃COO)₂·2H₂O was dissolved in 90 mL anhydrous ethanol. Then, 0.008 g sodium hydroxide was dissolved in 10 mL anhydrous ethanol solution to prepare sodium hydroxide ethanol solution (B solution). B solution was added to A solution under stirring at a volume ratio of 1/9. ZnO sol was obtained after aging for five days at room temperature. SnO₂ sol and ZnO sol were mixed in a volume ratio of 3/1. After aging for one day, SnO₂-ZnO composite sols were obtained. The SnO₂ or SnO₂-ZnO sols were coated on common glass substrates (30 mm × 20 mm × 1 mm) by dip-coating method. Appropriate amounts of B (0.05 mL 1.5 × 10⁻¹ mol·L⁻¹), Ag (0.05 mL 7 × 10⁻³ mol·L⁻¹), and F (0.05 mL 9 × 10⁻³ mol·L⁻¹) ions were doped into the surface layer of the SnO₂-ZnO composite films. In our experiment, the B, Ag, and F ions were doped into the surface layer via coating thin ions-doped sols onto the as-dried films. The prepared samples were heated at 550 °C in atmosphere for 1 h to induce the crystallization of particles.

3.2. Catalyst Characterization

The UV-Vis spectrophotometer (TU-1901, Beijing, China) equipped with an integrating sphere accessory (IS 19-1), using blank glass plate as a reference to analyze the light absorption, was used to record the diffuse reflectance spectra (DRS) of the films. The XRD profiles of the samples were recorded by X-ray diffraction with a diffractometer (AXS, Bruker, Germany). The phases and crystal sizes of the samples were measured with the 2θ range from 20 to 50° using Cu Kα radiation. The recombination of the electron-hole pairs was studied by the photoluminescence (PL, FLS920, Edinburgh, UK) emission spectra, which were recorded by a spectrometer with a 300 nm line of 450 W xenon lamps as an excitation source. The specific surface area, pore volume, and pore size distribution of the samples were analyzed by the nitrogen adsorption/desorption apparatus (ASAP2020, Microme, USA). The differential thermal analysis-thermogravimetry machine (DTA-TG, HCT-1, Beijing, China) was used in monitoring the crystallization behaviors in the temperature range 0–700 °C for obtaining the

DTA-TG curves of the samples. The surface morphology was characterized by high-resolution field emission scanning electron microscopy (SUPRA 55, ZEISS, Germany).

3.3. Catalyst Test

The degradation of methyl green ($16 \text{ mg}\cdot\text{L}^{-1}$) or formaldehyde ($5 \text{ mg}\cdot\text{L}^{-1}$) aqueous solution was used to value the photocatalytic activity of pure SnO_2 , $\text{SnO}_2\text{-ZnO}$, B doped $\text{SnO}_2\text{-ZnO}$, B/Ag di-doped $\text{SnO}_2\text{-ZnO}$, and B/Ag/F tridoped $\text{SnO}_2\text{-ZnO}$ films at ambient temperature. Each sample we tested was settled in 5 mL of methyl green or formaldehyde solution in a weighing bottle. The samples were stirred in the dark for 30 min to attain an adsorption/desorption equilibrium prior to light irradiation. A lamp equipped with UV cut-off filters ($\lambda > 400 \text{ nm}$) and a UV lamp (UV analyzer ZW-3, Jinan, China) with a wavelength of 365 nm were adopted as visible light and UV light sources, respectively. The degradation rate of the sample was assessed by the UV-Vis spectrophotometer (TU-1901). The formaldehyde is so hard to be detected directly due to its colorlessness that it should be determined by acetyl acetone spectrophotometry. The total error of the experiment was proved to be within the acceptable limit ($\pm 5\%$).

4. Conclusions

Environmental pollution, especially water pollution, is an urgent problem to be solved. In order to degrade all kinds of organic pollutants in sewage, we prepared B/Ag/F tridoped $\text{SnO}_2\text{-ZnO}$ composite films by a simple sol-gel method. As indicated by our experimental results, the photocatalyst significantly increased the degradation extent of various organic pollutants under both visible light and UV irradiations. A small amount of ZnO compositing and B/Ag/F tridoping played an important role in the photocatalytic activity of the film (wt%: Zn 0.95, B 1.28, Ag 2.34, F 0.82). The improved activity of the B/Ag/F tridoped $\text{SnO}_2\text{-ZnO}$ film is attributed to the low recombination rate of electron-hole pairs and strong absorption in visible light. The composite photocatalyst has potential application in industrial wastewater treatment.

Author Contributions: M.-M.Y. and K.H. conceived and designed the experiments; K.H. and X.-L.P. performed the experiments; F.L. analyzed the data; X.-L.P. contributed reagents/materials/analysis tools; M.-M.Y. and K.H. wrote the paper; all authors have read the final version of the manuscript.

Funding: This research received no external funding.

Acknowledgments: This work was financially supported partially by The Shandong Provincial Natural Science Foundation, China (ZR2016BM30).

Conflicts of Interest: The authors declare no conflict of interest.

References

1. Kumar, M.; Mehta, A.; Mishra, A.; Singh, J.; Rawat, M.; Basu, S. Biosynthesis of tin oxide nanoparticles using Psidium Guajava leave extract for photocatalytic dye degradation under sunlight. *Mater. Lett.* **2018**, *215*, 121–124. [[CrossRef](#)]
2. Patzsch, J.; Bloh, J.Z. Improved photocatalytic ozone abatement over transition metal-grafted titanium dioxide. *Catal. Today* **2018**, *300*, 2–11. [[CrossRef](#)]
3. Tsai, M.-T.; Chang, Y.-S.; Liu, Y.-C. Photocatalysis and luminescence properties of zinc stannate oxides. *Ceram. Int.* **2017**, *43*, S428–S434. [[CrossRef](#)]
4. Zheng, L.; Chen, C.; Zheng, Y.; Zhan, Y.; Cao, Y.; Lin, X.; Zheng, Q.; Wei, K.; Zhu, J. Photocatalytic activity of $\text{ZnO/Sn}_{1-x}\text{Zn}_x\text{O}_{2-x}$ nanocatalysts: A synergistic effect of doping and heterojunction. *Appl. Catal. B Environ.* **2014**, *148–149*, 44–50. [[CrossRef](#)]
5. Hoffmann, M.R.; Martin, S.T.; Choi, W.; Bahnemann, D.W. Environmental applications of semiconductor photocatalysis. *Chem. Rev.* **1995**, *95*, 69–96. [[CrossRef](#)]
6. Linsebigler, A.L.; Lu, G.; Yates, J.T. Photocatalysis on TiO_2 surfaces: Principles, mechanisms, and selected results. *Chem. Rev.* **1995**, *95*, 735–758. [[CrossRef](#)]

7. Houas, A.; Lachheb, H.; Ksibi, M.; Elaloui, E.; Guillard, C.; Herrmann, J.-M. Photocatalytic degradation pathway of methylene blue in water. *Appl. Catal. B Environ.* **2001**, *31*, 145–157. [[CrossRef](#)]
8. Jana, S.; Mitra, B.C.; Bera, P.; Sikdar, M.; Mondal, A. Photocatalytic activity of galvanically synthesized nanostructure SnO₂ thin films. *J. Alloy Compd.* **2014**, *602*, 42–48. [[CrossRef](#)]
9. Al-Hamdi, A.M.; Sillanpää, M.; Dutta, J. Photocatalytic degradation of phenol by iodine doped tin oxide nanoparticles under UV and sunlight irradiation. *J. Alloy Compd.* **2015**, *618*, 366–371. [[CrossRef](#)]
10. Masjedi-Arani, M.; Salavati-Niasari, M. Metal (Mn, Co, Ni and Cu) doped ZnO-Zn₂SnO₄-SnO₂ nanocomposites: Green sol-gel synthesis, characterization and photocatalytic activity. *J. Mol. Liq.* **2017**, *248*, 197–204. [[CrossRef](#)]
11. Ivetić, T.B.; Finčur, N.L.; Abramović, B.F.; Dimitrievska, M.; Štrbac, G.R.; Čajko, K.O.; Miljević, B.B.; Đaćanin, L.R.; Lukić-Petrović, S.R. Environmentally friendly photoactive heterojunction zinc tin oxide nanoparticles. *Ceram. Int.* **2016**, *42*, 3575–3583. [[CrossRef](#)]
12. Kong, X.-B.; Li, F.; Qi, Z.-N.; Qi, L.; Yao, M.-M. Boron-doped tin dioxide films for environmental applications. *Surf. Rev. Lett.* **2017**, *24*, 1750059. [[CrossRef](#)]
13. Hamrouni, A.; Moussa, N.; Parrino, F.; Di Paola, A.; Houas, A.; Palmisano, L. Sol-gel synthesis and photocatalytic activity of ZnO-SnO₂ nanocomposites. *J. Mol. Catal. A Chem.* **2014**, *390*, 133–141. [[CrossRef](#)]
14. Raj, N.P.M.J.; Rajesh, P.; Ramasamy, P.; Vijayan, N. One step synthesis of tin oxide nanomaterials and their sintering effect in dye degradation. *Optik* **2017**, *135*, 434–445.
15. Chiang, Y.-J.; Lin, C.-C. Photocatalytic decolorization of methylene blue in aqueous solutions using coupled ZnO/SnO₂ photocatalysts. *Powder Technol.* **2013**, *246*, 137–143. [[CrossRef](#)]
16. Ilkhechi, N.N.; Ghorbani, M.; Mozammel, M.; Khajeh, M. The optical, photo catalytic behavior and hydrophilic properties of silver and tin co doped TiO₂ thin films using sol-gel method. *J. Mater. Sci. Mater. Electron.* **2016**, *28*, 3571–3580. [[CrossRef](#)]
17. de Luna, M.D.G.; Laciste, M.T.; Tolosa, N.C.; Lu, M.C. Effect of catalyst calcination temperature in the visible light photocatalytic oxidation of gaseous formaldehyde by multi-element doped titanium dioxide. *Environ. Sci. Pollut. Res. Int.* **2018**, *25*, 15216–15225. [[CrossRef](#)] [[PubMed](#)]
18. Manikandan, A.S.; Renukadevi, K.B. Influence of fluorine incorporation on the photocatalytic activity of tin oxide thin films. *Mater. Res. Bull.* **2017**, *94*, 85–91. [[CrossRef](#)]
19. Li, H.; Zhang, W.; Guan, L.; Li, F.; Yao, M. Visible light active TiO₂-ZnO composite films by cerium and fluorine codoping for photocatalytic decontamination. *Mater. Sci. Semicond. Process.* **2015**, *40*, 310–318. [[CrossRef](#)]
20. Kong, X.; Li, F.; Qi, Z.; Qi, L.; Yao, M. SnO₂-based thin films with excellent photocatalytic performance. *J. Mater. Sci. Mater. Electron.* **2017**, *28*, 7660–7667. [[CrossRef](#)]
21. Li, F.; Yin, X.; Yao, M.; Li, J. Investigation on F-B-S tri-doped nano-TiO₂ films for the photocatalytic degradation of organic dyes. *J. Nanopart. Res.* **2011**, *13*, 4839–4846. [[CrossRef](#)]
22. Yamashita, H.; Harada, M.; Misaka, J.; Takeuchi, M.; Neppolian, B.; Anpo, M. Photocatalytic degradation of organic compounds diluted in water using visible light-responsive metal ion-implanted TiO₂ catalysts: Fe ion-implanted TiO₂. *Catal. Today* **2003**, *84*, 191–196. [[CrossRef](#)]
23. Al-Hamdi, A.M.; Sillanpää, M.; Dutta, J. Gadolinium doped tin dioxide nanoparticles: An efficient visible light active photocatalyst. *J. Rare Earths* **2015**, *33*, 1275–1283. [[CrossRef](#)]
24. Tang, W.; Wang, J.; Yao, P.-J.; Du, H.-Y.; Sun, Y.-H. Preparation, characterization and gas sensing mechanism of ZnO-doped SnO₂ nanofibers. *Acta Phys. Chim. Sin.* **2014**, *30*, 781–788.
25. Zhang, W.; Song, N.; Guan, L.; Li, F.; Yao, M. Photocatalytic degradation of formaldehyde by nanostructured TiO₂ composite films. *J. Exp. Nanosci.* **2015**, *11*, 185–196. [[CrossRef](#)]

